Available online at www.sciencedirect.com

ScienceDirect

Procedia Computer Science 00 (2018) 000–000

Procedia Computer Science

www.elsevier.com/locate/procedia

CENTERIS - International Conference on ENTERprise Information Systems / ProjMAN - International Conference on Project MANagement / HCist - International Conference on Health and Social Care Information Systems and Technologies, CENTERIS/ProjMAN/HCist 2018

Reformulating the Split-Spectrum Method to Facilitate the Estimation and Compensation of the Ionospheric Phase in SAR Interferograms

Urs Wegmüller, Charles Werner, Othmar Frey, Christophe Magnard, and Tazio Strozzi

Gamma Remote Sensing AG, Worbstrasse 225, CH-3073 Gümligen, Switzerland
http://www.gamma-rs.ch

Abstract

Spatial and temporal variation of the free electron concentration in the ionosphere affects SAR interferograms, in particular at low radar frequencies. The split-spectrum method permits separating the ionospheric and the non-dispersive phase terms using spectral sub-band images. In this work a reformulation of the split-spectrum method facilitates the necessary processing steps. Reformulating the split-spectrum method permits determining the ionospheric phase component based on a split-spectrum double-difference interferogram and the full-bandwidth differential interferogram. In this way differing a pair of unwrapped phase images, each one scaled by a large factor, can be avoided, making the method more robust. The applicability of the proposed method is demonstrated with examples including cases with very strong ionospheric effects.

Keywords: DInSAR; ionosphere; dispersive phase; non-dispersive phase; split-spectrum method; SSM, double difference interferogram;

* Corresponding author. Tel.: +41-31-9517005 ; fax: +41-31-9517008 .
E-mail address: wegmuller@gamma-rs.ch

1. Introduction

The SAR interferometric phase can be expressed as a sum of phase components including the flat earth phase, the topographic phase, the deformation phase, the atmospheric path delay phase and the ionospheric path delay phase. As described in [1], the ionospheric path delay phase, or in short ionospheric phase, can be expressed as

$$\phi_{iono} = \frac{4\pi K}{c f_0} \Delta TEC \tag{1}$$

where ΔTEC is the difference between the Total Electron Content (TEC) values integrated along the line-of-sight of the two radar acquisitions, and $K=40.31 m^3 s^{-2}$ is a constant, $c=3.0e08 m/s$ is the speed of light and f_0 is the radar center frequency. The ionospheric phase is proportional to $1/f_0$ and is called dispersive phase. All the other phase terms listed are proportional to f_0 and are called non-dispersive.

The concept of the split-spectrum approach is to determine separate interferograms for spectral sub-bands, permitting separation of the ionospheric and the non-dispersive phase terms ([2-8]). The ionospheric phase can be expressed as (see e.g. [6])

$$\phi_{iono} = \frac{f_L f_H}{f_0 (f_H^2 - f_L^2)} (\phi_L f_H - \phi_H f_L) \tag{2}$$

Where f_L and f_H are the radar center frequencies of the lower and higher spectral sub-bands and ϕ_L and ϕ_H are the interferometric phases of the lower and higher spectral sub-bands. Equation 2 expresses the ionospheric phase as a linear combination of the interferometric phases of the lower and higher spectral sub-bands. For a number of PALSAR 1 and PALSAR 2 modes Table 1 indicates the related factors *a* and *b* calculated using the lowest and highest third of the processed chirp spectrum for the lower and higher spectral sub-bands. As can be seen, the factors are non-integer values significantly larger than 1. To be able to apply these factors it is necessary to unwrap the lower and higher spectral sub-bands interferometric phases. Furthermore, significantly reducing phase noise through multi-looking and filtering, and avoiding phase unwrapping errors is required. For practical reasons we searched for ways to reduce the complexity of this task.

Table 1. Factors a and b used in $\phi_{iono} = a\phi_L + b\phi_H$ and x and z used in $\phi_{iono} = x\phi_0 + z(\phi_H - \phi_L)$ for PALASAR 1 and PALSAR 2 modes

Mode	*a*	*b*	*x*	*z*
PALSAR-1 FBS	34.27	-33.77	0.50	-34.02
PALSAR-1 FBD	68.29	-67.79	0.50	-68.04
PALSAR-2 SM1	12.12	-11.62	0.50	-11.83
PALSAR-2 SM2	24.65	-24.15	0.50	-24.40
PALSAR-2 SM3	37.50	-37.00	0.50	-37.25

The unwrapping and spatial filtering steps necessary to apply Eq. (2) are very delicate considering the relatively large factors *a* and *b* used to scale the two components. Using different spatial filters on a specific data set (e.g. different filter sizes or different weighting functions, or doing the filtering before or after the unwrapping etc.) can easily result in phase differences of 0.1 radian or larger. Scaling these with a factor around 34, for example, will result in phase differences larger than π. As demonstrated in the literature ([2-8]) the estimation of the ionospheric phase is possible using Eq. (2), if these steps are carefully performed and possibly including a step to identify and correct unwrapping errors as described in [6]. Nevertheless, increasing the robustness of the processing steps would be highly welcome and facilitate the applicability of the method.

In Section 2 we reformulate the split-spectrum method to increase the robustness of the necessary processing steps. In Section 3 we discuss a few aspects related to the implementation and application of the method. Then, in Section 4 application cases are presented, including one case with a relatively moderate ionospheric phase and two cases with very strong ionospheric effects caused by sporadic-E episodes as identified and analyzed in [7,9-11]. Section 5, finally, presents the conclusions.

2. Reformulating the split-spectrum method

With a simple algebraic transformation Equation 2 can be reformulated as a linear function of the full bandwidth interferometric phase and ϕ_0 (with center frequency f_0) and the split-spectrum double difference phase (ϕ_H - ϕ_L)

$$\phi_{iono} = x\phi_0 + z(\phi_H - \phi_L) \qquad \text{with} \quad x = \frac{f_L f_H}{f_0(f_H + f_L)} \quad \text{and} \quad z = -\frac{f_L f_H}{2f_0(f_H - f_L)} \tag{3}$$

For symmetrically chosen upper and lower spectral bands (i.e. $f_L = f_0 - \Delta f/2$ and $f_H = f_0 + \Delta f/2$) the x and z are

$$x = 0.5 - \frac{\Delta f^2}{8f_0^2} \approx 0.5 \quad \text{and} \quad z = -\frac{f_0}{2\Delta f} + \frac{\Delta f}{8f_0} \approx -\frac{f_0}{2\Delta f} \tag{4}$$

For a number of PALSAR 1 and PALSAR 2 modes Table 1 also indicates the factors *x* and *z*. As can be seen x has values very close to 0.5 (for the channels considered in Table 1 it differs from 0.5 by less than 0.001). This means the scale factor for the unwrapped interferometric phase is much smaller than in the original approach which is relevant concerning the scaling of noise effects and errors introduced in the filtering and unwrapping. The *z* factor is comparable in size to the *a* and *b* factors, but it is only applied to the split-spectrum double difference phase which is small compared to a phase cycle, so that unwrapping becomes trivial (unwrapping can be done to the lowest ambiguity).

Approximating *x* with 0.5 offers further possibilities. Multiplying both sides of Equation 3 we get

$$2\phi_{iono} = \phi_0 + 2z(\phi_H - \phi_L) \tag{5}$$

Unlike Equation 3 Equation 6 can also be applied to the wrapped ϕ_0. This means we can determine a complex valued image with the phase corresponding to twice the ionospheric phase. Generating this image permits to identify the level of ionospheric effects without having done an unwrapping for the interferogram (but only for the split-spectrum double difference interferogram). Furthermore, for pairs with a low level of ionospheric effects, which is expected to be the vast majority of interferometric pairs, unwrapping this $2\phi_{iono}$ should be trivial as long as the phases to unwrap remain in the interval $[-\pi,\pi]$.

Similarly, a complex valued image of twice the non-dispersive phase can be calculated by subtracting the scaled unwrapped split-spectrum double difference phase

$$2\phi_{non-dispersive} = 2\phi_0 - 2\phi_{iono} = \phi_0 - 2z(\phi_H - \phi_L) \tag{6}$$

Which means that a complex version of twice the ionospheric corrected interferogram can be generated without having done an unwrapping for the interferogram (but only for the split-spectrum double difference interferogram).

The interferometric phase is a sum of the ionospheric phase and the non-dispersive phase. Considering, that we are usually able to model and subtract orbital and topographic phase terms the main remaining phase terms in the non-dispersive phase are deformation phase and atmospheric path delay phase, besides error terms and phase noise.

So, especially at L-band, there are cases with rather low spatial variation in the non-dispersive phase. In such cases unwrapping twice the non-dispersive phase may be preferred over unwrapping the original interferogram.

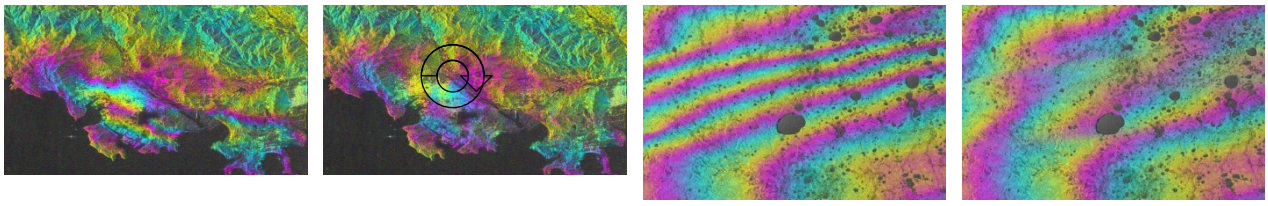

Fig. 1. Phase effects on L-band differential interferograms caused by co-registration errors in the presence of ionospheric path delay variations with strong along-track spatial gradients. (a) and (b) show a small section of the PALSAR-1 differential interferogram further discussed in Section 4.2. (c) and (d) show a small section of the PALSAR-2 differential interferogram further discussed in Section 4.3. The differential interferometric phase after co-registration using a carefully determined offset field is shown in (a) and (c). (b) and (d) show the same section of the same differential interferograms as obtained using a co-registration procedure with an offset polynomial.

Using Eq. 3 we call Method 1 (M1); besides calculating the unwrapped split-spectrum double difference phase the unwrapped phase of the differential interferogram needs to be calculated. Considering the full bandwidth instead of a sub-band has the advantage of a slightly higher coherence, but overall the complexity is the same as when using Eq. 2. The big advantage, though, is that the unwrapped phase is only scaled with a factor around 0.5 which strongly reduces the quality requirements. Using Eq. 5 we call Method 2 (M2) and using Eq. 6 we call Method 3 (M3). The obvious advantage of M2 and M3 is that complex-valued images of twice the ionospheric phase and twice the non-dispersive phase can be calculated requiring as the only unwrapping step the unwrapping of the split-spectrum double difference phase, which is, as mentioned before, straightforward. Provided twice the ionospheric phase or twice the non-dispersive phase can be unwrapped, permits also scaling to retrieve the unwrapped ionospheric and non-dispersive phases.

3. Processing related aspects

3.1. Band-pass filtering

In accordance with [3,7], we apply band-pass filtering along the range axis on the full-bandwidth SLCs considering the lowest and highest third of the processed bandwidth to get the lower and upper spectral sub-band SLCs. This band-pass filtering is done before the co-registration of the SLCs to avoid being affect by spectral shifts occurring in the resampling of the slave SLC as part of the co-registration. The sub-band SLCs are demodulated by applying a phase ramp to shift the spectrum to the center of the sampled spectrum and by changing the center frequencies to the new values.

3.2. SLC co-registration and effects of co-registration errors on the differential interferogram

Azimuth gradients in the ionospheric path delay can lead to azimuth positional offsets [12-14], at L-band of up to several SLC pixels. Applying a co-registration approach that is either exclusively based on the orbit data, SAR processing parameters and a digital elevation model (DEM), or that is based on offset low order polynomials determined using matching techniques, will provide an overall reasonable co-registration but will not compensate the local effects caused by the ionospheric path delay gradients. One effect of such registration errors of the order of a pixel is a significant reduction of the coherence. Furthermore, we observed, that registration errors can also significantly affect the interferogram phase. Two obvious examples of such effects are shown in Figure 1 using data that will be further discussed in Section 4. For the two sections shown the fringe pattern looks consistent for the more accurate co-registration with the offset field. Doing the co-registration with the less accurate offset polynomials results for areas affected by high ionospheric gradients in clearly different phase patterns. In fact, for the two sections shown this includes even “unreasonable phase patterns” such as closed paths on which the phase increases by 2π (see arrow in Fig. 1 image on top row to the right) and fringes that terminate (see center in Fig. 1

image on bottom row to the right). Our understanding of this effect is that non-linear ionospheric path delay changes within the synthetic aperture will cause some degradation of focus and a non-constant phase over the point. While the phase over a well-focused point target is constant it can show variation in azimuth direction when poorly focused. In the presence of positional mis-placements such gradients may then cause the observed phase offsets.

Our procedure to determine the co-registration offset field includes a first step based on the orbit, SAR parameters and DEM with a polynomial refinement to account for small overall offsets. In a second step residual offsets are determined using matching techniques. Based on the quality of the determined offsets and the spatial consistency of the offsets a conditioning of the offset field is applied e.g. to remove outliers, but also to interpolate the offset field in areas with poor coverage. The offset field is used to update the initial transformation lookup table and applied to get an improved co-registration. The quality of this co-registration is checked, and if necessary refined using a split-beam techniques. In the case of residual azimuth offsets the split-beam double difference phase will indicate the level of the residual offsets. Provided the previous refinement already reached in the azimuth direction a quality better than half an SLC pixel the unwrapping of the split-beam double difference phase becomes trivial as the values are in the interval $(-\pi,\pi)$. The unwrapped split-beam double difference phase are then scaled to azimuth offsets and used to update the co-registration transformation. Split-beam techniques can also be applied on a single SLC to identify which one of the two SLCs includes the ionospheric effects [14].

3.3. Role of spatial filtering and phase unwrapping

We use spatial filtering on one hand in support of the necessary phase unwrapping and on the other hand to reduce phase noise. Furthermore, spatial filtering is also used as a method to interpolate phase images across low coherence areas, e.g. to get a spatially more complete ionospheric path delay phase image. Filtering can be done both for the complex valued data sets and unwrapped phase images. To filter complex valued data we primarily use a modified Goldstein-Werner filter [15] as available in the Gamma Software [16]. For the spatial filtering of unwrapped phase images we use moving window filters with different filter seizes and weighting functions. For spatial phase unwrapping we use a minimum cost-flow (MCF) algorithm [17] implementation available in [16].

For more delicate cases, and interferograms with significant phase signals and spatially variable coherence are typically delicate cases, we often apply an iterative procedure to get an unwrapped, filtered phase. Initially stronger filtering is applied to get a spatial low-frequency component of the solution which is then subtracted from the complex valued image to get a differential complex valued image with reduced phase variations which may then be unwrapped more easily. Once the phase variations remain within the interval $(-\pi,\pi)$ the complex valued interferogram can directly be converted to a unwrapped phase image independent of the noise level. This permits then to do the filtering on the unwrapped phases. Along the process quality control is important to avoid errors being introduced by phase unwrapping problems.

In the processing of the results presented in Section 4 we worked at a relatively high spatial resolution with multi-looked pixel sizes of the order of 20m. The spatial resolution of the estimated ionospheric phase is significantly lower than this as spatial filters are used. Furthermore, it is relevant that the SAR signal for a specific pixel is acquired along a full synthetic aperture which covers a significant along-track section of the ionosphere.

4. Data examples

4.1. Palsar-2 over Tokyo harbor area

As a first example we selected a PALSAR-2 L-band pair acquired at HH-polarization in SM1 mode with a relatively moderate ionospheric phase. While this may be less challenging what concerns accomplishing the necessary processing steps and less interesting what concerns the study of ionospheric effects cases as this one and cases with even lower ionospheric effects are the vast majority of cases encountered when working with satellite InSAR. Calculating either an offset field or a split-beam interferogram [18,19] indicates that the pair is not affected by high ionospheric path delay gradients. Based on this we decided to use a co-registration approach without determining and applying an additional offset field correction estimated based on the data. The split-spectrum double differential interferogram was determined considering the lowest and highest third of the available processed

range bandwidth using 6 range and 5 azimuth looks in the multi-looking. The complex valued split-spectrum double differential interferogram was spatially filtered and unwrapped by a simple conversion of the phases to be within the interval (-π,π). Methods 1 to 3 were then applied and the results are shown in Fig. 2.

The original interferogram shows an overall phase ramp of about one phase cycle across the image and additional local phase variations. The estimated ionosphere corresponds quite well to the overall phase ramp. Based on our experience from other interferograms over the same area we interpret the large scale part of the estimated non-dispersive phase mainly as atmospheric. All 3 methods presented are applicable and result in very similar results. To correct the ionospheric effects using Method 1 does not really have disadvantages over the other methods in this case as unwrapping the differential interferogram was not found more complicated than unwrapping twice the ionospheric phase or twice the non-dispersive phase. Methods 2 and 3 offer the possibility, though, to get a good qualitative idea of the ionospheric and non-dispersive phases without unwrapping anything besides the split-spectrum double differential interferogram.

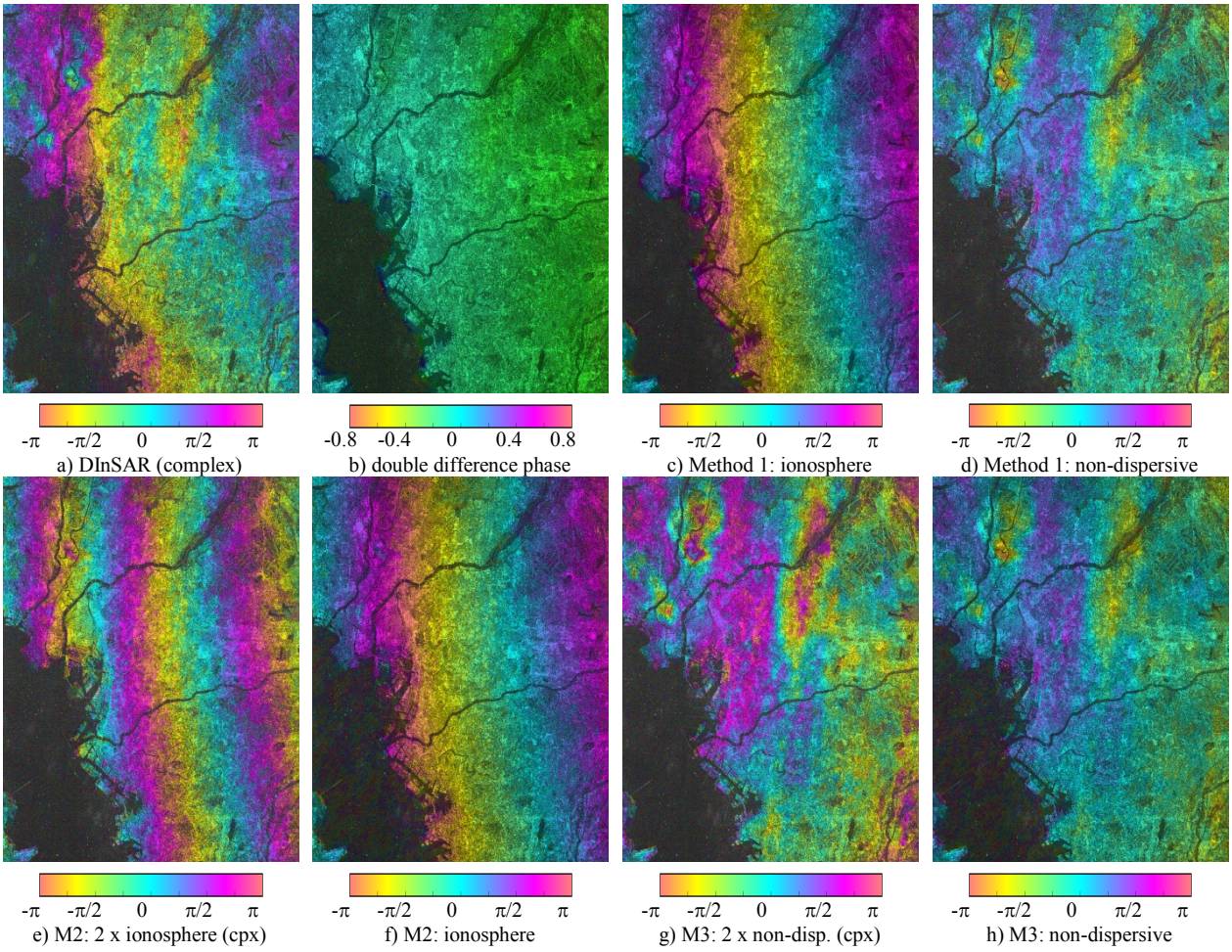

Fig. 2. Estimation and compensation of ionospheric path delay for PALSAR-2 HH-pol. SM1 mode data acquired on 8-Sep-2016 and 1-Dec-2016 over Tokyo harbor area. The data of a full frame is shown in slant range geometry. The upper line shows (a) the differential interferogram, (b) the split-spectrum double difference phase, (c) the ionospheric path delay estimated using Eq (3), and (d) the non-dispersive phase calculated by subtracting (c) from (a). The lower line shows (e) twice the ionospheric phase derived using Method 2, (f) the corresponding ionospheric phase, (g) twice the non-dispersive phase derived using Method 3 and (h) the corresponding non-dispersive phase. To facilitate cross-comparison the same cyclic color scale is used to visualized the wrapped (a,e,g) and unwrapped phases (b,c,d,f,h).

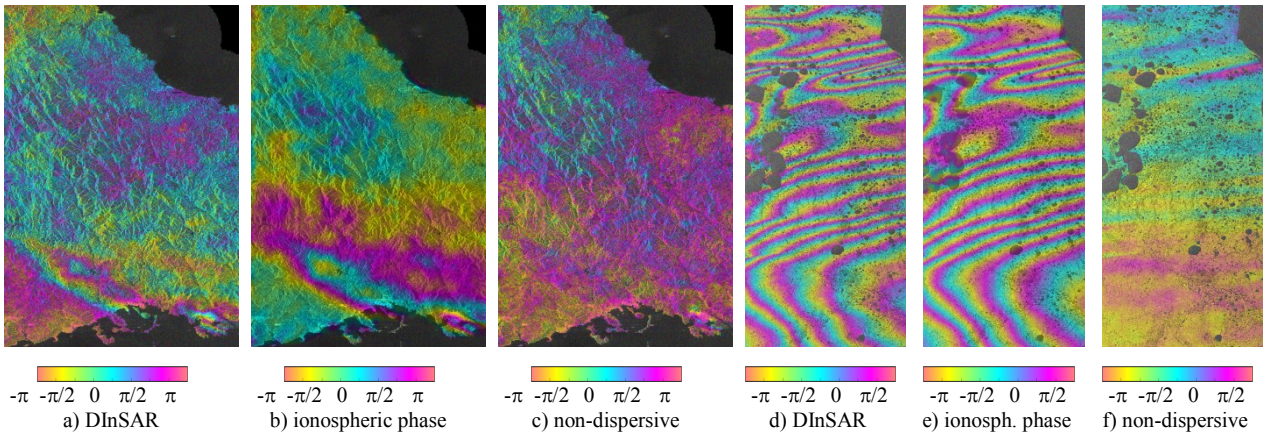

Fig. 3. Estimation and compensation of ionospheric path delay for PALSAR-1, path 72, frames 2920-2930, HH-pol. FBS mode data acquired on 28-Mar-2009 and 28-Jun-2009 over Yamaguchi Prefecture, Japan (a-c) and PALSAR-2, path 156, frames 1400-1420, HH-pol. SM3 mode data acquired on 17-Aug-2015 and 14-Sep-2015 over the Yamal Peninsula in Northern Siberia (d-f). To facilitate cross-comparison the same cyclic color scale is used to visualized the wrapped (a,d) and unwrapped phases (b,c,e,f).

4.2. Palsar-1 over Yamaguchi Prefecture, Japan

The data used is the same as used in the first example discussed in [7], i.e. a case with very strong ionospheric effects caused by sporadic-E episodes as identified and analyzed in [7,9-11]. The data analyzed covers two full frames. In the processing we applied much care to achieve a good co-registration using an iterative improvement of the offset field as described in Section 3.2. The differential interferogram as well as the estimated ionospheric phase and the "ionosphere-corrected" non-dispersive phase are shown in Fig. 3. Overall Method 1 worked well. Only in the area at the lower right corner (shown also in Fig. 1) we observe in the non-dispersive phase local patterns that correlate with the location of the highest ionospheric gradients present in the pair which are most likely related to an imperfect compensation of the ionospheric phase. While [7] states that it was necessary to consider higher order ionospheric phase terms to get a good compensation of the ionospheric phase, we obtained a good result by just considering the first order ionosphere effect.

4.3. Palsar-2 over data over Yamal Peninsula in Northern Siberia, Russia

This case corresponds to the first case in the additional material provided in [7], an example with very strong ionospheric effects. The same processing as for the example described in Section 4.2 was used. For an area covered by 3 subsequent PALSAR-2 frames acquired in SM3 mode the differential interferogram as well as the estimated ionospheric phase and the "ionosphere-corrected" non-dispersive phase are shown in Fig. 4. In comparison to [7] the result is much less noisy in areas with large gradients in the ionospheric phase, as a combination of using the reformulated method presented that does not require a scaling of the unwrapped interferometric phase with a large factor and a more accurate co-registration. The ionosphere-corrected interferogram (non-dispersive phase) shows good coherence for the entire land surface. The phase variation observed correlates with the ionospheric phase and includes therefore most likely residual ionospheric phase, possibly caused by still imperfect co-registration or higher order effects in the presence of very high ionospheric phase gradients.

5. Conclusions

Slightly reformulating the split-spectrum method permitted determining the ionospheric phase component based on the split-spectrum double difference interferogram and the full bandwidth differential interferogram. The main advantage of this method is that scaling with a large factor is only necessary for the unwrapped split-spectrum double difference interferogram phase. Estimating the unwrapped split-spectrum double difference interferogram

phase is quite straightforward and robust as the phases are in the interval ($-\pi,\pi$). A second advantage is that the unwrapped phase of the full-bandwidth interferogram is used for the second term instead of a sub-band interferogram, which increases the robustness of the unwrapping and filtering.

Furthermore, it was shown that complex valued images of twice the ionospheric phase and twice the non-dispersive phase can be derived requiring only the unwrapping of the split-spectrum double-difference interferogram. This is useful to check the presence and level of ionospheric effects in a pair. It also offers further possibilities in cases difficult to unwrap. In cases with a complicated non-dispersive fringe pattern, e.g. relating to an earthquake, the image of twice the ionospheric phase may confirm that the level of ionospheric effects is not very strong. Consequently, twice the ionospheric phase can be unwrapped and the interferogram can be corrected for the ionospheric effects without unwrapping the original.

The applicability of the proposed methods was demonstrated with 3 examples including two with very strong ionospheric effects.

References

[1] Meyer, F., Bamler, R., Jakowski, N., Fritz, T., (2006). The potential of low-frequency SAR systems for mapping ionospheric TEC distributions. IEEE Geosci. Remote Sens. Lett. 3, 560–564. http://dx.doi.org/10.1109/LGRS.2006.882148.

[2] Brcic, R., Parizzi, A., Eineder, M., Bamler, R., Meyer, F., (2010). Estimation and compensation of ionospheric delay for SAR interferometry. In: Geoscience and Remote Sensing Symposium (IGARSS), 2010 IEEE International. IEEE, pp. 2908–2911.

[3] Brcic, R., Parizzi, A., Eineder, M., Bamler, R., Meyer, F., (2011). Ionospheric effects in SAR interferometry: An analysis and comparison of methods for their estimation. In: Geoscience and Remote Sensing Symposium (IGARSS), 2011 IEEE International. IEEE, pp. 1497–1500.

[4] Rosen, P.A., Hensley, S., Chen, C., (2010). Measurement and mitigation of the ionosphere in L-band interferometric SAR data. In: Radar Conference, 2010 IEEE. IEEE, pp. 1459–1463.

[5] Gomba, G., De Zan, F., (2015). Estimation of ionospheric height variations during an aurora event using multiple semi-focusing levels. In: 2015 IEEE International Geoscience and Remote Sensing Symposium (IGARSS). IEEE, pp. 4065–4068.

[6] Gomba, G., Parizzi, A., De Zan, F., Eineder, M., Bamler, R., (2016). Toward operational compensation of ionospheric effects in SAR interferograms: the split-spectrum method. IEEE Trans. Geosci. Remote Sens. 54, 1446–1461.

[7] Furuya M., Suzuki T., Maeda J., and Heki K., (2017). Midlatitude sporadic-E episodes viewed by L-band split-spectrum InSAR, Earth Planets and Space (2017) 69:175; https//doi.org/10.1186/s40623-017-0764-6.

[8] Liao H., Meyer F.J., Scheuchl B., Mouginot J., Joughin I., and Rignot E., (2018). Ionospheric correction of InSAR data for accurate ice velocity measurement at polar regions, Remote Sensing of Environment, 209 (2018) pp. 166-180, https://doi.org/10.1016/j.rse.2018.02.048.

[9] Maeda J, Heki K (2014). Two-dimensional observations of midlatitude sporadic E irregularities with a dense GPS array in Japan. Radio Sci 49:28–35. https://doi.org/10.1002/2013RS005295.

[10] Maeda J, Heki K (2015) Morphology and dynamics of daytime mid-latitude sporadic-E patches revealed by GPS total electron content observations. Earth Planets Space 67:89. https://doi.org/10.1186/s40623-015-0257-4.

[11] Maeda J, Suzuki T, Furuya M, Heki K (2016) Imaging the midlatitude sporadic E plasma patches with a coordinated observation of spaceborne InSAR and GPS total electron content. Geophys Res Lett 43:1419–1425. https://doi.org/10.1002/2015GL067585.

[12] Gray A.L. D.E. Mattar, and G. Sofko, (2000). Influence of ionospheric electron density fluctuations on satellite radar interferometry, Geophys. Res. Letters, Vol. 27, No. 10, pp. 1451-1454, 2000.

[13] Meyer F., R. Bamler, N. Jakowski, and T. Fritz, (2005)., The potential of broadband L-band SAR systems for small scale ionospheric TEC mapping, Procs. FRINGE 2005 Workshop, Frascati, Italy, 28. Nov. - 2 Dec., 2005 (http://earth.esa.int/workshops/fringe2005).

[14] Wegmüller U., C. Werner, T. Strozzi, and A. Wiesmann, (2006). „Ionospheric electron concentration effects on SAR and INSAR", Proc. IGARSS 2006, Denver, Colorado, USA, 31- Jul. – 4. Aug. 2006.

[15] Goldstein R M, Werner C L., (1998). Radar interferogram filtering for geophysical applications [J]. Geophysical Research Letters, 1998, 25(21):4035–4038.

[16] Gamma Software Information (2018) at https://www.gamma-rs.ch/software.html

[17] M. Costantini, (1998). "A novel phase unwrapping method based on network programming," IEEE Trans. Geosci. Remote Sens. Vol. 36, 1998, pp. 813 -8.

[18] Bechor N. and H. Zebker, (2006). Measuring two-dimensional movements using a single InSAR pair, GRL Vol. 33, L16311, 2006.

[19] Wegmüller U., T. Strozzi, and C. Werner, (2012). Ionospheric path delay estimation using split-beam interferometry, Procs. IGARSS'2012, Munich, Germany, 22-27 July 2012.